Biochimica et Biophysica Acta 1807 (2011) 262–269

Contents lists available at ScienceDirect

Biochimica et Biophysica Acta

journal homepage: www.elsevier.com/locate/bbabio

Kinetics and energetics of electron transfer in reaction centers of the photosynthetic bacterium *Roseiflexus castenholzii*

Aaron M. Collins [b], Christine Kirmaier [b], Dewey Holten [b], Robert E. Blankenship [a,b,*]

[a] Department of Biology, Washington University in St. Louis, St. Louis, MO 63130, USA
[b] Department of Chemistry, Washington University in St. Louis, St. Louis, MO 63130, USA

ARTICLE INFO

Article history:
Received 24 September 2010
Received in revised form 18 November 2010
Accepted 19 November 2010
Available online 29 November 2010

Keywords:
Reaction center
Electron transfer
Cytochrome
Roseiflexus castenholzii

ABSTRACT

The kinetics and thermodynamics of the photochemical reactions of the purified reaction center (RC)-cytochrome (Cyt) complex from the chlorosome-lacking, filamentous anoxygenic phototroph, *Roseiflexus castenholzii* are presented. The RC consists of L- and M-polypeptides containing three bacteriochlorophyll (BChl), three bacteriopheophytin (BPh) and two quinones (Q_A and Q_B), and the Cyt is a tetraheme subunit. Two of the BChls form a dimer P that is the primary electron donor. At 285 K, the lifetimes of the excited singlet state, P*, and the charge-separated state $P^+H_A^-$ (where H_A is the photoactive BPh) were found to be 3.2 ± 0.3 ps and 200 ± 20 ps, respectively. Overall charge separation $P^* \rightarrow\rightarrow P^+Q_A^-$ occurred with ≥90% yield at 285 K. At 77 K, the P* lifetime was somewhat shorter and the $P^+H_A^-$ lifetime was essentially unchanged. Poteniometric titrations gave a P_{865}/P_{865}^+ midpoint potential of +390 mV vs. SHE. For the tetraheme Cyt two distinct midpoint potentials of +85 and +265 mV were measured, likely reflecting a pair of low-potential hemes and a pair of high-potential hemes, respectively. The time course of electron transfer from reduced Cyt to P^+ suggests an arrangement where the highest potential heme is not located immediately adjacent to P. Comparisons of these and other properties of isolated *Roseiflexus castenholzii* RCs to those from its close relative *Chloroflexus aurantiacus* and to RCs from the purple bacteria are made.

1. Introduction

Roseiflexus (*Rfl.*) *castenholzii* is a niche-adapted, filamentous anoxygenic phototroph (FAP) that lacks chlorosomes, the primary light-harvesting architecture in green bacteria [1]. Light-harvesting is realized only in the membrane antenna (B800–880) complex which is in close association with a RC. Bacteriochlorophyll (BChl) and carotenoids within the antenna complex are organized in a similar manner to the B808–866 complex from *Chloroflexus* (*Cfl.*) *aurantiacus* but also share many spectroscopic and functional similarities to light-harvesting 1 and light-harvesting 2 complexes from purple bacteria [2–4].

Excitation captured by the antenna complex is rapidly and efficiently transferred to a photochemical RC. The RC is an integral membrane, pigment-protein complex that uses light excitation to facilitate charge separation across the membrane. The RC from purple bacteria is comprised of L- and M-polypeptide subunits and A- and B-branches of cofactors, respectively, with a pseudo-C_2 symmetry axis. An additional H-subunit resides on the cytoplasmic side of the complex. The cofactor arrangement in the RC of purple bacteria is shown in Fig. 1 with identical cofactors along each branch of the RC, with the exception that some species utilize different quinones. However, remarkably, charge separation is unidirectional along the A-branch. The RC from *Cfl. aurantiacus* shares similarities with the purple bacterial RC, however it differs most significantly in containing three BChl and three BPh, and in being comprised of only the L- and M- polypeptides (i.e., lacking the H polypeptide of the purple bacterial RC) [5,6]. The cofactor arrangement in *Cfl. aurantiacus* RCs is generally thought to be as in Fig. 1 with the third BPh presumed to replace B_B [5,7]. While there is no definitive proof where the third BPh resides, circumstantial evidence that it occupies the B_B site comes from sequence alignments of the (putative) L- and M- polypeptides in comparison to the L- and M- polypeptides of purple bacterial RCs. These alignments indicate that in *Cfl. aurantiacus* and *Rfl. castenholzii*: (1) the His residue that serves as an axial ligand to B_B (residue M180 in *B. viridis* and *Rb. capsulatus*, and M182 in *Rb. sphaeroides*) is leucine and isoleucine, respectively, and (2) the His at L153, which serves as the ligand to B_A, is preserved [8,9]. Furthermore, The L- and M-subunits of *Rfl. castenholzii* show relatively high homology

Abbreviations: RC, reaction center; FAP, filamentous anoxygenic phototroph; BChl, bacteriochlorophyll; BPh, bacteriopheophytin; P, primary electron donor; B_A and B_B, monomeric BChls on the A and B-branches, respectively; H_A and H_B, BPhs associated with the A- and B-branches respectively; Q_A and Q_B, quinones associated with the A- and B-branches, respectively; Cyt, RC-associated cytochrome complex; LDAO, lauryldimethylamine N-oxide; TA, transient absorption; E_{m8}, midpoint potential at pH = 8; *E*h, ambient redox potential

* Corresponding author. Departments of Biology and Chemistry, Washington University in St. Louis, St. Louis, MO 63130, USA. Tel.: +1 314 935 7971; fax: +1 314 935 5125.
E-mail address: Blankenship@wustl.edu (R.E. Blankenship).

0005-2728/$ – see front matter © 2010 Elsevier B.V. All rights reserved.
doi:10.1016/j.bbabio.2010.11.011

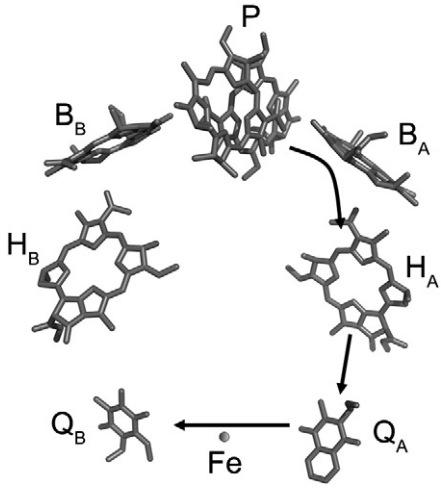

Fig. 1. Cofactor arrangement in the RC from purple bacteria (PDB accession: PDB ID: 2PRC). The RC Cyt subunit and cofactors are not shown. Electron transfer in the RC is along the A-branch of cofactors and is indicated with arrows. The cofactors are: P—the primary electron donor; B_A and B_B—the accessory BChls along the A- and B-branches, respectively; H_A and H_B—the BPhs along the A- and B-branches, respectively; Q_A and Q_B are menaquinone and ubiquinone, respectively. In *Cfl. aurantiacus* (and presumably *Rfl. castenholzii*), a BPh is thought to occupy the B_B site, both quinones are menaquinone and the non-heme Fe is replaced by Mn.

to the analogous L- and M-polypeptides of *Cfl. aurantiacus* (52% and 44%, respectively) [9]. These observations suggest a similar structure.

The kinetics of electron transfer in the RC from several species of purple bacteria, including many mutants, have been extensively studied (for review see [10]). At room temperature, the excited singlet state of the dimeric primary electron donor, P^*, transfers an electron to B_A (~3–4 ps) which, on a sub-picosecond timescale, then transfers an electron to H_A. A superexchange mechanism of electron transfer may also contribute, as has been demonstrated for electron transfer from P^* to H_B, albeit with slower time constants [11–14]. Regardless, the characteristic spectral features of $P^+H_A^-$ form on the 3–4 ps timescale. Electron transfer of $P^+H_A^- \rightarrow P^+Q_A^-$ occurs with a time constant of about 200 ps. The P^* and $P^+H_A^-$ lifetimes are 1–2 ps and 100 ps, respectively, at cryogenic temperatures [15]. The overall conversion of $P^* \rightarrow\rightarrow P^+Q_A^-$ occurs with essentially 100% yield [16,17] and is followed by electron transfer to Q_B on the μs time scale. After two successive turnovers of RC photochemistry, Q_B has received two electrons and picked up two protons forming the quinol, Q_BH_2, which diffuses out of the RC and is replaced by a new quinone from the membrane pool. Very similar charge separation processes occur in *Cfl. aurantiacus* RCs, (see [18] for a review). At room temperature, the P^* lifetime is ~7 ps and the time constant for $P^+H_A^- \rightarrow P^+Q_A^-$ is ~300 ps [19,20] with overall charge separation of ~100% yield [21]. At cryogenic temperatures, the P^* lifetime becomes markedly multiexponential [22].

Electron donation to P^+ is achieved in purple bacterial RCs either by a small soluble cytochrome (Cyt) or an RC-attached tetraheme Cyt depending on species (see [23,24]). In the latter situation, the individual hemes are arranged as alternating pairs having high and low potentials. Altogether, the four hemes span a range of about −80mV to +350 mV, as in *Blastochloris* (*B.*) *viridis* [25,26]. Moreover, all four hemes in *B. viridis* have slightly different α-band absorption maxima [26]. *Cfl. aurantiacus* RCs contain a tetraheme Cyt subunit, however, it readily dissociates from the RC during purification [27]. In membrane fragments, as well as the purified Cyt complex, four potentiometrically distinct *c*-type hemes can be resolved. However, the individual hemes appear to be spectroscopically identical [27]. The Cyt complex in *Cfl. aurantiacus* also appears to span a more narrow range (0 to 300 mV) [27,28]. *Rfl. castenholzii* RCs are isolated with a bound tetraheme Cyt [9].

Here we present the kinetics and energetics of electron transfer in RCs from *Rfl. castenholzii* determined using pump/probe absorption difference spectroscopy and potentiometric titrations of the bound tetraheme Cyt complex and of P_{865}/P_{865}^+. The measured kinetics and redox potentials are somewhat intermediary between what is observed in the well-studied purple bacterial RCs and the RC from *Cfl. aurantiacus*. Comparisons are made between both phototrophic groups.

2. Materials and methods

2.1. Reaction center purification

RCs were purified from cells of *Rfl. castenholzii* as described previously [2] with the exception that the detergent lauryl dimethylamine N-oxide (LDAO) was used in every step of the purification. The RCs used in the studies reported here had 280/816 nm absorbance ratios ≤ 2.5 in a final buffer composition of 0.1% LDAO and 100 mM NaCl in 20 mM Tris buffer (pH = 8.0). RC samples were either prepared fresh or stored at −80 °C until used.

2.2. Redox titrations

Potentiometric titrations on purified RCs were performed in the dark using a thin layer quartz glass spectroelectrochemical cell with a Pt gauze working electrode. Ag-AgCl/3 M KCl was used as the reference electrode and was calibrated against a saturated solution of quinhydrone at various pH values. All potentials are stated relative to the standard hydrogen electrode (SHE). The potential was controlled by a CH620 C potentiostat (CH Instruments Inc.). At each potential, the RC absorption spectrum (375–900 nm) was recorded following sample equilibration for several minutes. Oxidative and reductive titrations were performed with 65 mM KCl and 20 μM of the following mediators to accelerate the equilibrium between the working electrode and the RCs: potassium ferricyanide, N,N,N′,N′-tetramethyl-1,4-phenylenediamine (DAD), 2,3,5,6-tetramethyl-p-phenylenediamine (TMPD), phenazine ethosulfate, phenazine methosulfate, 2-hydroxy-1,4-anthroquinone, 1,2-napthoquinone, 1,2-napthoquinone-4-sulfonic acid and 2-methyl-1,4-naphthoquinone (menadione). Data were fit to $n = 1$ Nernst curves and multiple redox titrations yielded midpoint values within ±10 mV for all titrations.

2.3. Spectroscopy

Flash-induced absorption changes on the ns to s time regimes were measured on an Edinburgh Instruments LP920 flash photolysis spectrometer. Excitation flashes (FWHM of 6 ns) at 590 nm were generated by a Q-switched Nd:YAG laser at a repetition rate of 0.033 Hz. Kinetics were monitored at 605 nm. The instrument temporal resolution was < 10 ns. RCs (3 μM) were mixed with 20 μM of the mediators listed above as well as 4 mM o-phenanthroline to prevent electron transfer from Q_A to Q_B [29]. The ambient redox potential was adjusted by small (~1 μL) additions of 100 mM sodium ascorbate or potassium ferricyanide and the solution potential was followed by an Ag/AgCl electrode.

Ultrafast transient absorption measurements were performed on a system described previously [30,31]. Samples (2.5–3 mL of 25–35 μM RCs) were flowed from an ice-cooled reservoir through a 2 mm path length cuvette, maintaining a sample temperature of ~285 K. For measurements at 77 K, RCs were mixed with an equal volume of glycerol, placed in a home-built acrylic cuvette (~2 mm path length) and frozen in the dark in an Oxford Instruments CF1204 cryostat. For all experiments, the excitation energy was attenuated so that a single flash excited < 30% of the RCs in the pump/probe region. At 77 K and when using 605 nm excitation flashes, a ~1% systematic decrease in the magnitude of the absorption changes per transient absorption (TA) spectrum was observed. (Each TA spectrum is the result of ~90

flashes at 10 Hz.) The original magnitude could be restored by moving the cryostat to a fresh pump/probe region; however, a quantitative study of the P-bleaching and stimulated emission using 605-nm excitation was not possible. Sample/signal degradation did not occur when using 870 nm excitation flashes at 77 K, and time constants of the primary photochemistry reported here are based on spectral/kinetic data acquired between 500 and 700 nm. Global analysis of the ps spectral evolution to determine kinetic components was performed using Origin Data Analysis and Graphing Software (Version 8.1; Origin Labs) and home-written fitting routines consisting of the convolution of the instrument response (overlap of pump and probe flashes) and one or more exponentials plus a constant.

2.4. Pigment extraction and quantification

Pigments from purified RCs were extracted and quantified by high-performance liquid chromatography (HPLC) essentially as described previously [2]. Briefly, concentrated RCs were completely extracted with ice cold 8:2 (v/v) methanol/acetone and the RC pigments were separated by reverse-phase HPLC using a 100% methanol mobile phase. Under these conditions, BChl and BPh were separated by several minutes. BChl and BPh were monitored at 770 nm and 750 nm, respectively and the area under each elution peak was integrated. The extinction coefficient for BChl *a* in methanol was taken to be 60 cm^{-1} mM^{-1} at 770 nm [32]. The extinction coefficient for BPh *a* in methanol was determined to be 36 cm^{-1} mM^{-1} at 750 nm by converting a sample of BChl to BPh by adding 1/200 vol of concentrated HCl to the sample in a manner similar to that described by Straley et al. [33].

3. Results

3.1. Ground-state absorption and pigment quantification

The pigment content of the RC was verified by pigment extraction as described above and yielded a BChl/BPh ratio of 1:1 (data not shown) which is in accord with the pigment content of 3 BChl and 3BPh in the isolated *Cfl. aurantiacus* RC [5,6]. The ground state spectra of *Rfl. castenholzii* RCs at 295 and 77 K are shown in Fig. 2. The purified RC does not contain carotenoid. The spectral features are very similar to those reported previously for *Rfl. castenholzii* RC membrane preparations [9] and for isolated *Cfl. aurantiacus* RCs [6,34]. The near infrared Q_Y absorption bands at 864, 816 and 760 nm (295 K) can be assigned to P, monomeric B_A and the three BPhs, respectively, and are in 0.6 : 1.0 : 1.0 ratio. The Q_X transitions of all the BChl coalesce at 605 nm. The ~500–550 nm region has contributions from the Q_X bands of the BPhs and the RC-associated Cyt and were better resolved in the 77 K spectra (see below). The Soret band of the Cyt has a strong peak around 415 nm while the peaks at 392 and 365 nm are the overlapping Soret bands of the BChls and BPhs.

At 77 K, the Q_Y absorption of P red-shifts to 887 nm and a new feature resolved at 788 nm is likely the upper exciton band of the special pair as suggested previously for *Cfl. aurantiacus* RCs at 4 K [35]. The inset of Fig. 2 shows features between 500 and 550 nm that are resolved at 77 K. The two peaks at 542 and 532 nm can be assigned to the Q_X bands of the BPhs. In *Cfl. aurantiacus* RCs, the Q_x bands of BPh are resolved into two distinct bands at 4 K [36]. The peak at 552 nm and shoulder around 524 nm are attributed to the α- and β-bands of the Cyt, respectively. This assignment is corroborated by the redox titrations presented below.

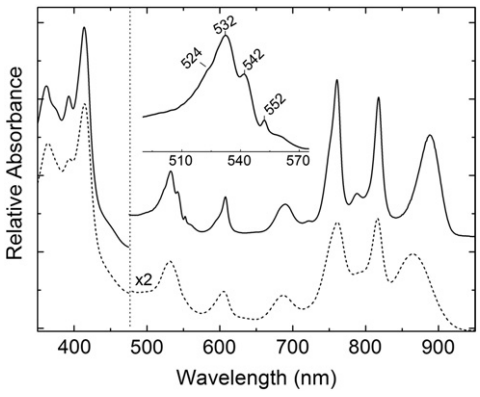

Fig. 2. Absorption spectra of isolated RCs from *Rfl. castenholzii* at ambient potential: 295 K (dashed) and 77 K (solid). The 77 K spectrum has been offset for clarity; both spectra have been multiplied by 2 at wavelengths >475 nm. The inset expands the spectrum between 500 and 575 nm with peak wavelengths noted. Other absorbance maxima are given in the text.

3.2. Potentiometric titrations of the RC

Redox titrations of P, monitored as a change in absorption at 865 nm as a function of applied potential are shown in Fig. 3A. The data were fit to an $n=1$ Nernst curve with a midpoint potential of +390 mV at pH = 8.0 (Fig. 3A, red curve). This value is similar to the midpoint of P/P^+ measured in *Cfl. aurantiacus* isolated RCs (+386 mV) [37] or cytoplasmic membranes (+362 mV) [29]), and is about 100 mV lower than the P/P^+ potential found in most purple bacterial RCs. The potentials of the Cyt hemes were evaluated similarly by monitoring absorbance changes in the α-band at 553 nm. The titration was fit best to the sum of two $n=1$ Nernst curves with potentials of+85 and

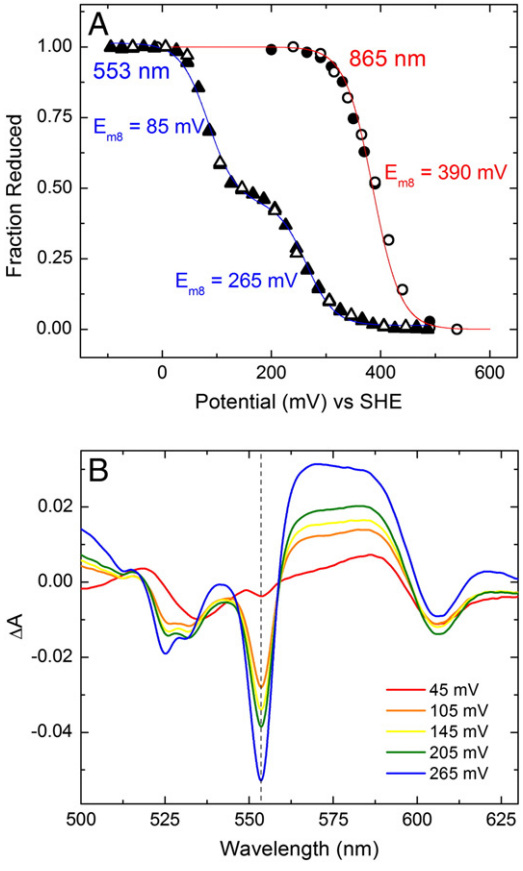

Fig. 3. (A) Potentiometric titration of the *Rfl. castenholzii* RC. The optical absorption of the primary donor, P, (865 nm, circles) and the α-band of the Cyt subunit (553 nm, triangles) were monitored as a function of reduction potential. Closed and opened symbols represent oxidative and reductive titrations, respectively. The data were fit (solid lines) to a Nernst equation for the titration of P, or the sum of two Nernst equations in the case of the Cyt α-band. The midpoint potentials (pH = 8) are given (E_{m8}). (B) To highlight the small absorption changes in the α-band at several different potentials, difference spectra between the potential tested and the fully reduced sample are shown.

+265 mV (Fig. 3A, blue curve). The relative amplitudes of the two components are 0.55 and 0.45, respectively, indicating nearly equal contributions from the two potential waves. A similar titration of the absorption changes of the β-band of the Cyt at 524 nm yielded potentials within the uncertainty limits of the α-band titration (result not shown).

The sequence of *Rfl. castenholzii* Cyt indicates the presence of four hemes [9] as is the case of many of Cyt associated with purple bacterial RCs [24]. These data suggest that the *Rfl. castenholzii* Cyt is comprised of "pairs" of high and low potential hemes. Moreover, all four hemes of the Cyt studied here are spectroscopically identical; regardless of the potential tested, a single α-band was observed at 553 nm as indicated in the series of spectra in Fig. 3B, which plot the difference between the spectrum at the potential tested and the spectrum of the fully reduced sample (Fig. 3B). The occurrence of a single α-band peak was previously observed for Cyt-554 from *Cfl. aurantiacus*, however, the Cyt complex was purified separately from the RC and midpoint potentials of 0, +120, +220 and +300 mV vs. SHE were measured for the four hemes [27].

3.3. Kinetics of electron donation between tetraheme cytochrome and P^+

The kinetics of electron donation from the tetraheme Cyt to the oxidized special pair was monitored at 295 K at different reduction potentials. Fig. 4 shows representative kinetics traces that monitored the Q_X band of P at 605 nm. At +330 mV the Cyt should be fully oxidized. 6-ns non-saturating excitation flashes centered at 590 nm and at a repetition rate of 0.033 Hz were used to induce the formation of P^+ as measured by bleaching at 605 nm. The decay of this bleaching could be fit by the sum of two exponentials: a dominant kinetic component of 42 ms (80% relative amplitude) and a second, smaller component >10 s (20% relative amplitude). We assign the 42 ms component to charge recombination between P^+ and Q_A^-, in agreement with the time constant for $P^+Q_A^-$ charge recombination (~50–60 ms) in *Cfl. aurantiacus* RCs [5,38]. The >10 s component probably represents long-lived charge recombination between Cyt^+ and Q_A^- however, activity of residual Q_B cannot be ruled out despite the addition of *o*-phenanthroline to the sample. At a potential of +290 mV, where only one high potential heme should be reduced, the kinetics could be fit to a dual-exponential function of 3.3 μs (83% relative amplitude) and 42 ms (17% relative amplitude) components. The 3.3 μs component likely represents the reduction of P^+ by one of the high potential hemes and, based on the results given above, the 42 ms component can be ascribed to $P^+Q_A^-$ charge recombination in residual RCs having the Cyt fully oxidized. When the potential was poised at +230 mV, where both high potential hemes should be >75% reduced, the 42-ms component was abolished and two new fast components were observed. The time profile was fit to the sum of two exponentials, giving values of 530 ns (89% relative amplitude) and 3.3 μs (11% relative amplitude). The 530 ns component likely represents reduction of P^+ by the second high potential heme. When the potential was poised at +170 mV where both high potential hemes should be reduced, a single 480 ns kinetic component was sufficient to fit the data; the 480 ns value is in good agreement with the 530-ns value measured at +230 mV potential.

The reduction of P^+ by the Cyt alternatively could be monitored via appearance of bleaching of the Cyt α-band at 553 nm. For example, when the reduction potential was poised at +170 mV, the bleaching at 553 nm developed with a dominant 470-ns component (82% relative amplitude)

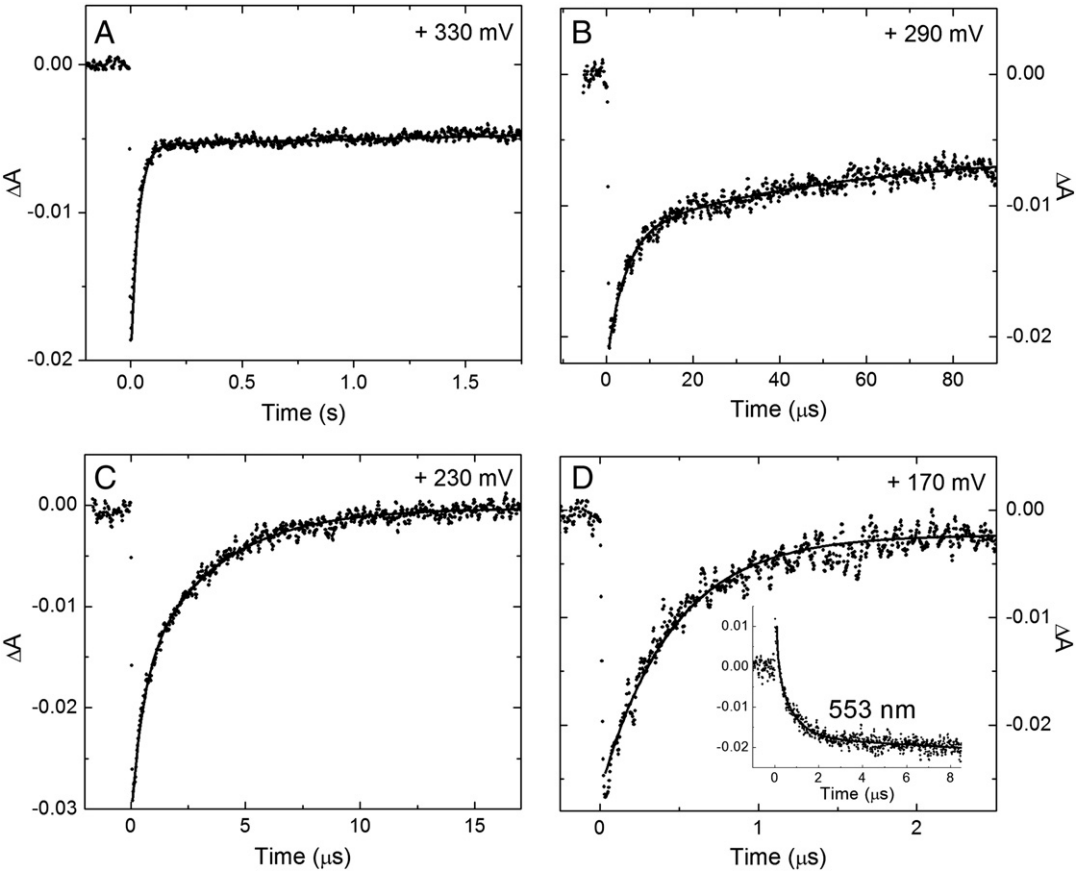

Fig. 4. Representative time profiles of electron transfer on the ns to s timescales. A 6 ns (FWHM), non-saturating, laser pulse at 590 nm was used to excite the sample at a repetition of 0.033 Hz while transients were monitored at 605 nm. Each trace is the average of 20 flashes. The redox potential was poised at $E_h = +330$ mV (A), $E_h = +290$ mV (B), $E_h = +230$ mV and $E_h = +170$ mV (D) vs SHE. The inset in D shows kinetics monitored in the 553-nm cytochrome α-band at a redox potential of +170 mV. Solid lines are exponential fits to the kinetic traces and are described further in the text.

and a minor component (18% relative amplitude) of ~2 μs (Fig. 4D, inset). The value of the fast component is in excellent agreement with that determined from the P band at 605 nm and +170 mV. The 2 μs component might reflect electron transfer between hemes of the cytochrome complex.

3.4. Primary charge separation processes

Fig. 5 shows 285 K TA spectra taken at key times following excitation of *Rfl. castenholzii* RCs with 130 fs flashes. These spectra parallel spectra acquired at similar times for purple bacterial RCs such as *Rb. capsulatus* or *Rb. sphaeroides* [15,39], or RCs from *Cfl. aurantiacus* [19,20]. The transient states and key spectral features can be assigned as follows: (1) for P* (black spectra at 0.5 ps), featureless absorption between 500 and 700 nm with bleaching of the P ground state bands at 605 and 860 nm and stimulated emission from P* at ~850–980 nm; (2) for $P^+H_A^-$ (red spectra at 20 ps), bleaching of P at 605 and 860 nm, bleaching of the Q_X band of H_A at 542 nm and the H_A anion bands at 662 nm and 943 nm; and (3) for $P^+Q_A^-$ (blue spectra at 3 ns), nearly featureless absorption between 500 and ~580 nm and bleaching of the P bands at 605 and 860 nm. The small band-shift like feature near 550 in the 3 ns spectrum is present in the spectra of purple bacterial RCs also and is thought to be an electrochromic shift (likely associated with a BPh) in response to formation of P^+; this feature is resolved better at low temperature where it can be seen clearly in both the $P^+H_A^-$ and $P^+Q_A^-$ spectra (as in [40] and see also Fig. 7 below).

The spectra in Fig. 5 show that overall $P^* \rightarrow\rightarrow P^+Q_A^-$ conversion occurs with very high yield as reflected in the nearly constant magnitude of P bleaching as a function of time. For example, consider the magnitude of 605 nm bleaching *relative* to the positive P* or P^+ absorption at 580–590 in the 0.5 ps, 20 ps and 3 ns spectra (Fig. 5A). In the near infrared band of P (Fig. 5B), stimulated emission contributes to the TA spectrum and may manifest at or near the 860 nm maximum of the P bleaching, one cannot rule out ~10% decay of P* to the ground state; however, there is little change in the bleaching magnitude on the blue side (830–850 nm) of the P band (Fig. 5B). The data thus support ≥90% overall $P^* \rightarrow\rightarrow P^+H_A^- \rightarrow P^+Q_A^-$ charge separation in *Rfl. castenholzii* RCs with no evidence for electron transfer to the B-branch to within 10%. Data sets spanning 500–700 nm and −5 ps to 3.8 ns, and spanning 830–980 nm and −5 ps to 3.8 ns, were fit by global analysis to the convolution of two pulses plus two exponentials plus a constant. This returned values of 3.2 ± 0.3 ps for the P* lifetime and 200 ± 20 ps for the $P^+H_A^-$ lifetime. Representative data and fits in two individual 10-nm intervals are shown in Fig. 6. The ~3 ps and ~200 ps lifetimes determined are similar to those found for *Rb. capsulatus* and *Rb. sphaeroides* [41] RCs and somewhat shorter than the ~7 ps and ~300 ps found for *Cfl. aurantiacus* RCs [19,22].

The P* spectrum in the visible region at 77 K (0.5 ps spectrum in Fig. 7A) is very similar to that at 285 K (Fig. 5A). Bleaching of the near-infrared Q_Y band of P and P* stimulated emission (elicited by 600-nm excitation; data not shown) both are shifted to longer wavelengths as routinely observed in purple bacterial RCs. Formation of $P^+H_A^-$ at 77 K is rapid, giving rise to some bleaching of the Q_X band of H_A at 543 nm in the spectrum acquired at 0.5 ps. This bleaching along with the H_A anion band at 665 nm are fully developed by 20 ps (red $P^+H_A^-$ spectrum, Fig. 7). The similar magnitude of the 600-nm P bleaching in the P* and $P^+H_A^-$ spectra indicate that the yield of $P^* \rightarrow P^+H_A^-$ is ≥85%. Limited assessment of the Q_Y P bleaching magnitude (using 600 nm flashes; see Materials and methods) confirms a high yield of charge separation (data not shown). The shoulder on the blue side of the 543-nm H_A bleaching likely represents an electrochromic shift as discussed above. The spectra at later times (500 ps and 3 ns, Fig. 7) reveal that about one-third of $P^+H_A^-$ persists—i.e., has not decayed to form $P^+Q_A^-$.

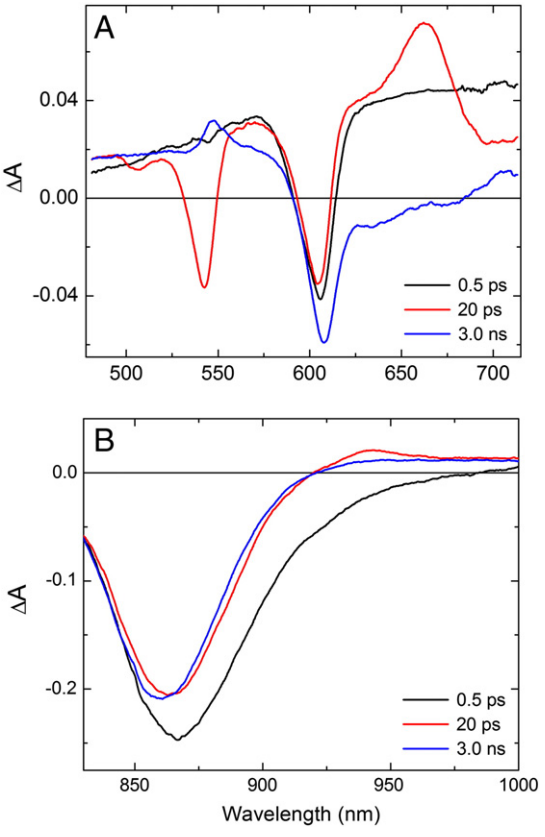

Fig. 5. Transient absorption difference spectra acquired at 285 K at various times after a 130-fs excitation flash at 860 nm (A) or 605 nm (B).

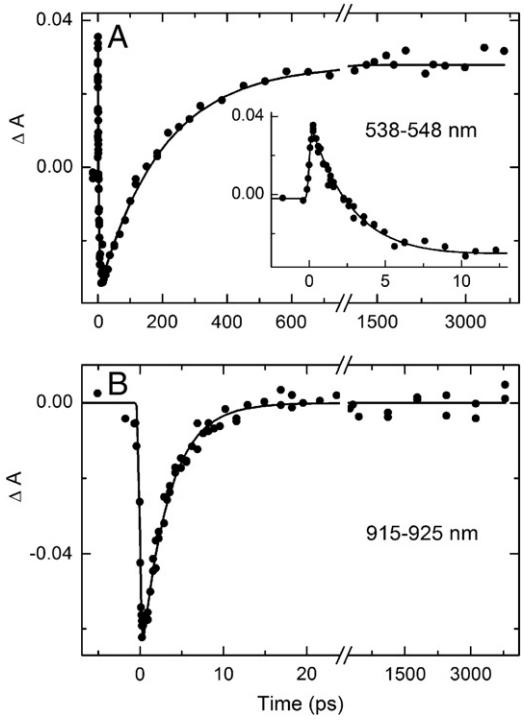

Fig. 6. (A) Absorption changes averaged between 538 and 548 nm (circles) for the appearance and decay of bleaching of the Q_X band of H_A, and fit (solid line) to the convolution of the instrument response and two exponentials (3.2 and 195 ps) plus a constant. (B) Stimulated emission decay data, averaged between 915 and 925 nm (circles), and fit (solid line) to the convolution of the instrument response and one exponential (3.2 ps) plus a constant. The inset shows the same data on a shorter time scale. The excitation conditions were as in Fig. 5. The fit time constants are those obtained from global analysis and correspond well to those derived from fits to the data at the two individual wavelength intervals shown.

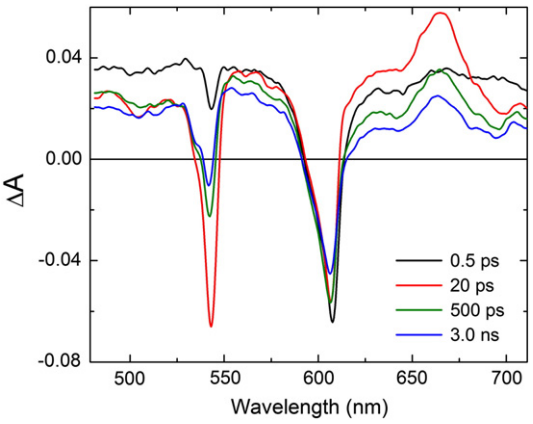

Fig. 7. Transient absorption difference spectra obtained at 77 K at various times after 130 fs excitation at 870 nm.

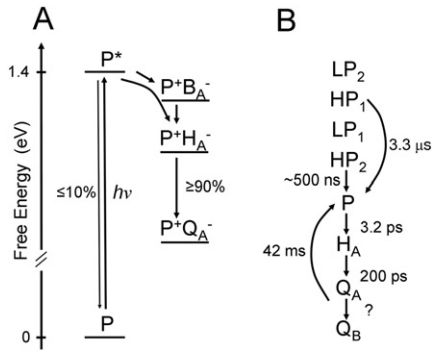

Fig. 8. (A) Schematic energy level and yield diagram for the *Rfl. castenholzii* RC at 285 K. (B) Kinetics of electron transfer among various RC cofactors determined in this work. An alternating high, low, high, low pattern for the heme arrangement is proposed. HP_1 and HP_2 are the highest and second highest potential hemes, respectively, and LP_1 and LP_2 are the two lower potential hemes.

From this we deduce that in about one-third of the *Rfl. castenholzii* RCs used here at 77 K, Q_A is inactive (is reduced, missing, or has perhaps moved to a non-functional position). In this fraction we expect that $P^+H_A^-$ decays in tens of ns via charge recombination to the ground state and formation of triplet P. In the other two-thirds fraction, $P^+H_A^-$ appears to decay via ~200 ps electron transfer to Q_A as described below. Overall at 77 K, the initial electron transfer steps in the RC parallel those measured at 285 K, with no clear evidence of electron transfer to the B-branch of cofactors.

Data spanning 500–700 nm and −5 ps to 3.8 ns were fit by global analysis to the convolution of the instrument response plus three exponentials plus a constant, with the third component added (compared to the analysis at 285 K) for the $P^+H_A^-$ lifetime in the ~one-third fraction with inactive Q_A. In purple bacterial RCs at 90–100 K when Q_A is pre-reduced or depleted, the $P^+H_A^-$ lifetime is 20 ns [42] or 21 ns [43], respectively. In the global analysis here, the time constant of one component was fixed at various values between 5 and 30 ns. Regardless of the value (5 to 30 ns), the fit values of the other two time constants were 1.9 ± 0.2 ps and 200 ± 20 ps. These results show that the P* lifetime is shorter in *Rfl. castenholzii* RCs at 77 K than at 285 K (3 ps), as also seen for purple bacterial RCs ([10] and refs. therein). On the other hand the $P^+H_A^-$ lifetime at 77 K is the same within experimental error as that found at 285 K. In purple bacterial RCs the 77 K lifetime is about a factor of two shorter [15] and in *Cfl. aurantiacus* it is to our knowledge unknown.

The time profiles at 77 K were also globally fit to a function consisting of the instrument response convolved with four exponentials plus a constant. One component was again fixed at 5–30 ns (for the Q_A inactive fraction), and the other (fit) components had time constants of ~1 ps, ~8 ps and ~200 ps, with the latter again reflecting the $P^+H_A^-$ lifetime. We associate the two faster components to P* based on the globally-derived amplitude spectra (not shown), with the 1 and 8 ps components having relative amplitudes about 80% and 20%, respectively. Multi-exponential P* decays or wavelength-dependent time constants in RCs are widely reported and a variety of molecular origins involving static and dynamic heterogeneity have been discussed.

4. Discussion

We have presented here kinetics and energetics of electron transfer in the isolated RC from *Rfl. castenholzii*. From our results and with adoption of certain equivalencies to the well-studied purple bacterial RCs, schematic free energy and kinetic diagrams are presented in Fig. 8. The compositions and photochemistry of *Rfl. castenholzii* and *Cfl. aurantiacus* RCs have both strong similarities to and differences from each other and purple bacterial RCs. Some of these have been described above. We will highlight a few additional comparisons. X-ray crystal structures of purple bacterial RCs show that there is a hydrogen bond between a conserved Glu at L104 and the $C13^1$-keto group of H_A. This is the main (but not sole) source of the difference between the position of the Q_X bands of H_A and H_B. For example, in wild type *Rb. capsulatus* these bands are at 542 nm (H_A) and 528 nm (H_B). In the L104-Gln and L104-Leu mutants, the Q_X band of H_A is at 540 and 531 nm, respectively [44]. Putative sequence alignments of *Rfl. castenholzii* and *Cfl. aurantiacus* position a Gln at the equivalent residue of L104. The TA data clearly show that the photoactive BPh absorbs at 542 nm. Together, these comparisons are consistent with the presumed model that the L-polypeptide of *Rfl. castenholzii* is the equivalent of the "photoactive" L- or A-branch of the purple bacteria RC.

The two other BPhs in *Rfl. castenholzii* both appear to have Q_X absorption near 530 nm, though the exact positions are likely masked by the Cyt absorption. One of these BPhs is presumably the equivalent of H_B, and the other BPh (which we will denote Φ_B) has been suggested to occupy the B_B site as described in the Introduction. A BChl in the B_A site would make the cofactor arrangement along the A-branch of the RC identical to wild type RCs from purple bacteria and is consistent with our observation of essentially wild type-like primary charge separation for *Rfl. castenholzii*, and for *Cfl. aurantiacus* previously [20,22]. A conundrum exists nonetheless because BPh is 200–300 mV easier to reduce than BChl *in vitro* [45], making Φ_B a potent electron acceptor. This exact situation was tested by Katilius et al. [46] who replaced the His ligand to B_B at M182 in *Rb. sphaeroides* with Leu. This resulted in the incorporation of a BPh, Φ_B, in place of B_B, a P* lifetime of 2.8 ± 0.1 ps and $35 \pm 5\%$ electron transfer from P* to Φ_B [46]. $P^+\Phi_B^-$ was found to have a lifetime of 200 ± 20 ps and to decay by charge recombination to the ground state. In other words, $P^+\Phi_B^-$ is a trap for electron transfer on the B-side in this *Rb. sphaeroides* mutant. Clearly there are differences in the local environments of Φ_B in the *Rb. sphaeroides* mutant, *Rfl. castenholzii* and *Cfl. aurantiacus* that must account for these differences. Very recently, Pudlak and Pincak [47] calculated that unidirectional electron transfer in the RC from *Cfl. aurantiacus* could be accounted for by including differences in the electronic coupling between the two branches of cofactors. However, in the RC from the purple bacterium, *Rb. sphaeroides*, asymmetry of electron transfer was prominently due to the differences in free energy between the two branches of cofactor [47].

Another interesting point is that in purple bacterial RCs, a conserved Tyr-M208 (*B. viridis and Rb. capsulatus* numbering) in proximity to P, B_A and H_A is key in enabling rapid charge separation to the A-branch via lowering the energy of the $P^+B_A^-$ state [48]. Mutation of this residue to Leu results in a significant slowing of the time constant for the formation of $P^+H_A^-$ [49–51]. Similarly, changing the Phe to a Tyr at the C_2-symmetry related cite L181 (in proximity to P, B_B and H_B) facilitates electron transfer to H_B [11,13]. Leu is found at M208 in the *Cfl. aurantiacus*

RC and this difference has been suggested to explain the slower ~7 ps kinetics of initial charge separation [22,52]. However, *Rfl. castenholzii* RCs also have Leu at M208 yet the P* lifetime is ~3 ps.

Another distinction in the amino acids around the cofactors in *Rfl. castenholzii* and *Cfl. aurantiacus* compared to purple bacterial RCs affects the P/P^+ potential. This potential is considerably influenced by hydrogen bonds to the keto carbonyl and acetyl groups of the two BChls that comprise P [53]. Wild-type RCs from purple bacteria have a P/P^+ midpoint potential of ~500 mV and a single H-bond between His-L168 and the acetyl group of the L-side BChl *a* of P. Replacement of this residue with Phe results in a decrease of the P/P^+ potential to 410 mV while addition of H-bonds increases the potential [53–55]. In *Rfl. castenholzii* and *Cfl. aurantiacus*, there is a Phe at L168 (again identified by putative sequence alignment), and the P/P^+ potential in the latter is appreciably lower [29,37]. Consistent with these findings, we find a P/P^+ midpoint potential of 390 mV for *Rfl. castenholzii*. A slightly lower P/P^+ midpoint potential but a similar Q_Y ground state absorption maximum for P (865 nm) might reflect P^* being slightly easier to oxidize in *Rfl. castenholzii* RCs than in purple bacterial RCs.

Redox titration of the α- and β-bands of the RC-bound tetraheme Cyt-*c* of *Rfl. castenholzii* reveals two waves that were successfully fitted to the sum of two Nernst ($n=1$) equations giving +85 and +265 mV. These likely reflect a pair of high- and a pair of low-potential hemes. Early measurements on the RC Cyt subunits from *B. viridis* [56] and *Chromatium vinosum* [57] suggested that the Cyt probably contained four hemes; however, only two different potentials were measured. Later it was shown in *B. viridis* that the α-band of each heme absorbs at a slightly different wavelength and that the hemes are potentiometrically distinct [26]. The Cyt of *Cfl. aurantiacus*, which does not co-purify with the RC, contains 4 hemes with similar spectral properties but with unique midpoint potentials [27]. The spectral and potentiometric analysis of *Rfl. castenholzii* Cyt revealed that the four hemes have similar spectral properties. However, only two distinct redox potentials were resolved, each of which corresponds to two hemes.

The kinetics of electron transfer between the RC Cyt subunit and P^+ revealed that when only the highest potential heme was reduced prior to the flash, P^+ was reduced with a time constant of 3.3 μs. When both high-potential hemes are reduced, a single exponential of ~500 ns is sufficient to describe kinetics of electron donation to P^+. A simple correlation of rate and distance suggests that the second highest-potential heme is closest to P (labeled HP_2 in Fig. 8B). We tested the cytochrome oxidation and P^+ reduction at $E_h = 0$ mV where all four of the hemes are reduced prior to the flash and observed a single exponential decay of <350 ns (results not shown). This suggests that one of the low potential hemes (LP_1 or LP_2) is also located near P thus making HP_1 located in the third or fourth position in the complex (Fig. 8B). While this contrasts from the heme arrangement for the RC of *B. viridis* where the highest potential heme is located immediately adjacent to P [25,26], a similar model was predicted for the tetraheme Cyt of *Roseobacter denitrificans* [58], *Chromatium vinosum* [59] and *Rubrivivax gelatinosus* [60]. When one of the hemes in the cytochrome subunit from *Cfl. aurantiacus* was reduced prior to the excitation flash, P^+ was reduced with a half-time of 1.4 μs [61]. When the other hemes in the complex were subsequently reduced, the rate of electron donation to P^+ was progressively increased. The rise in rate was attributed to an electrostatic influence on HP_1 which was also suggested to reside nearest to P. This study and the results presented here suggest that the heme arrangement in *Rfl. castenholzii* might be different than that of *Cfl. aurantiacus*.

In summary, it appears that RCs from FAPs as well as purple bacteria both perform asymmetric electron transfer despite having very similar branches of cofactors. In both cases, the terminal electron acceptor quinone (Q_B) requires two successive electron turnovers of the RC (and two protons) to become fully reduced before diffusing out of the RC. Control of electron flow through only one branch of RC cofactors would thus serve to reduce the possibility of fruitless charge recombination. Unidirectional electron transfer is also manifested in PSII from plants and algae that also contain a terminal quinone acceptor. Finally, the energetics and kinetics of the primary photochemistry in *Rfl. castenholzii* RCs appear to have similarities to both *Cfl. aurantiacus* and purple bacteria. High-resolution structural data for an FAP RC would be useful to delineate the structural differences between FAPs and purple bacteria.

Acknowledgments

This work was supported by Grants MCB-0646621 to R.E.B., and MCB-0948996 to C.K. and D.H., from the Molecular Biochemistry Program of NSF. The authors gratefully acknowledge Dr. Dariusz Niedzwiedzki for the determination of the BPhe extinction coefficient.

References

[1] N.-U. Frigaard, D. Bryant, in: J.M. Shively (Ed.), Complex Intracellular Structures in Prokaryotes, Springer, Berlin Heidelberg, 2006, pp. 79–114.
[2] A.M. Collins, P. Qian, Q. Tang, D.F. Bocian, C.N. Hunter, R.E. Blankenship, Light-harvesting antenna system from the phototrophic bacterium *Roseiflexus castenholzii*, Biochemistry 49 (2010) 7524–7531.
[3] A.M. Collins, Y. Xin, R.E. Blankenship, Pigment organization in the photosynthetic apparatus of *Roseiflexus castenholzii*, Biochim. Biophys. Acta 1787 (2009) 1050–1056.
[4] D.M. Niedzwiedzki, A.M. Collins, A.M. LaFountain, M.M. Enriquez, H.A. Frank, R.E. Blankenship, Spectroscopic studies of carotenoid-to-bacteriochlorophyll energy transfer in LHRC photosynthetic complex from *Roseiflexus castenholzii*, J. Phys. Chem. B 114 (2010) 8723–8734.
[5] R.E. Blankenship, R. Feick, B.D. Bruce, C. Kirmaier, D. Holten, R.C. Fuller, Primary photochemistry in the facultative green photosynthetic bacterium *Chloroflexus aurantiacus*, J. Cell. Biochem. 22 (1983) 251–261.
[6] B.K. Pierson, J.P. Thornber, Isolation and spectral characterization of photochemical reaction centers from the thermophilic green bacterium *Chloroflexus aurantiacus* strain J-10-f1, Proc. Natl Acad. Sci. USA 80 (1983) 80–84.
[7] A. Ivancich, R. Feick, A. Ertlmaier, T.A. Mattioli, Structure and protein binding interactions of the primary donor of the *Chloroflexus aurantiacus* reaction center, Biochemistry 35 (1996) 6126–6135.
[8] Y.A. Ovchinnikov, N.G. Abdulaev, B.E. Shmuckler, A.A. Zargarov, M.A. Kutuzov, I.N. Telezhinskaya, N.B. Levina, A.S. Zolotarev, Photosynthetic reaction centre of *Chloroflexus aurantiacus* primary structure of M-subunit, FEBS Lett. 232 (1988) 364–368.
[9] M. Yamada, H. Zhang, S. Hanada, K.V.P. Nagashima, K. Shimada, K. Matsuura, Structural and spectroscopic properties of a reaction center complex from the chlorosome-lacking filamentous anoxygenic phototrophic bacterium *Roseiflexus castenholzii*, J. Bacteriol. 187 (2005) 1702–1709.
[10] J. Wachtveitl, W. Zinth, in: B. Grimm, R. Porra, W. Rüdiger, H. Scheer (Eds.), Chlorophylls and Bacteriochlorophylls, Springer Netherlands, Dordrecht, 2006, pp. 445–459.
[11] J.I. Chuang, S.G. Boxer, D. Holten, C. Kirmaier, High yield of M-side electron transfer in mutants of *Rhodobacter capsulatus* reaction centers lacking the L-side bacteriopheophytin, Biochemistry 45 (2006) 3845–3851.
[12] B.A. Heller, D. Holten, C. Kirmaier, Control of electron transfer between the L- and M-sides of photosynthetic reaction centers, Science 269 (1995) 940–945.
[13] C. Kirmaier, C. He, D. Holten, Manipulating the direction of electron transfer in the bacterial reaction center by swapping Phe for Tyr near BChlM (L181) and Tyr for Phe near BChlL (M208), Biochemistry 40 (2001) 12132–12139.
[14] C. Kirmaier, D. Weems, D. Holten, M-Side Electron transfer in reaction center mutants with a lysine near the nonphotoactive bacteriochlorophyll, Biochemistry 38 (1999) 11516–11530.
[15] C. Kirmaier, D. Holten, W.W. Parson, Temperature and detection-wavelength dependence of the picosecond electron-transfer kinetics measured in *Rhodopseudomonas sphaeroides* reaction centers. Resolution of new spectral and kinetic components in the primary charge-separation process, Biochim. Biophys. Acta 810 (1985) 33–48.
[16] J. Breton, J.L. Martin, A. Migus, A. Antonetti, A. Orszag, Femtosecond spectroscopy of excitation energy transfer and initial charge separation in the reaction center of the photosynthetic bacterium *Rhodopseudomonas viridis*, Proc. Natl Acad. Sci. USA 83 (1986) 5121–5125.
[17] W. Holzapfel, U. Finkele, W. Kaiser, D. Oesterhelt, H. Scheer, H.U. Stilz, W. Zinth, Initial electron-transfer in the reaction center from *Rhodobacter sphaeroides*, Proc. Natl Acad. Sci. USA 87 (1990) 5168–5172.
[18] FeickR. , ShiozawaJ.A. , ErtlmaierA. , in: BlankenshipR.E. , MadiganM.T. , Bauer (Eds.), Anoxygenic Photosynthetic Bacteria, Kluwer Academic Publishers, Dordrecht, 1995.
[19] Y. Xin, S. Lin, R.E. Blankenship, Femtosecond spectroscopy of the primary charge separation in reaction centers of *Chloroflexus aurantiacus* with selective excitation in the Q_Y and Soret bands, J. Phys. Chem. A 111 (2007) 9367–9373.
[20] C. Kirmaier, R.E. Blankenship, D. Holten, Formation and decay of radical-pair state P^+I^- in *Chloroflexus aurantiacus* reaction centers, Biochim. Biophys. Acta 850 (1986) 275–285.

[21] M. Volk, G. Scheidel, A. Ogrodnik, R. Feick, M.E. Michel-Beyerle, High quantum yield of charge separation in reaction centers of *Chloroflexus aurantiacus*, Biochim. Biophys. Acta 1058 (1991) 217–224.
[22] M. Becker, V. Nagarajan, D. Middendorf, W.W. Parson, J.E. Martin, R.E. Blankenship, Temperature dependence of the initial electron-transfer kinetics in photosynthetic reaction centers of *Chloroflexus aurantiacus*, Biochim. Biophys. Acta 1057 (1991) 299–312.
[23] H. Axelrod, O. Miyashita, M. Okamura, in: C.N. Hunter, F. Daldal, M.C. Thurnauer, J.T. Beatty (Eds.), The Purple Phototrophic Bacteria, Springer, Dordrecht, 2009, pp. 323–336.
[24] W. Nitschke, S.M. Dracheva, Reaction center associate cytochromes, in: R.E. Blankenship, M.T. Madigan, C.E. Bauer (Eds.), Anoxygenic Photosynthetic Bacteria, 1995, pp. 775–805.
[25] W. Nitschke, A.W. Rutherford, Tetraheme cytochrome c subunit of *Rhodopseudomonas viridis* characterized by EPR, Biochemistry 28 (1989) 3161–3168.
[26] S.M. Dracheva, L.A. Drachev, A.A. Konstantinov, A.Y. Semenov, V.P. Skulachev, A.M. Arutjunjan, V.A. Shuvalov, S.M. Zaberezhnaya, Electrogenic steps in the redox reactions catalyzed by photosynthetic reaction-centre complex from *Rhodopseudomonas viridis*, Eur. J. Biochem. 171 (1988) 253–264.
[27] J.C. Freeman, R.E. Blankenship, Isolation and characterization of the membrane-bound cytochrome c-554 from the thermophilic green photosynthetic bacterium *Chloroflexus aurantiacus*, Photosynth. Res. 23 (1990) 29–38.
[28] P. van Vliet, D. Zannoni, W. Nitschke, W.A. Rutherford, Membrane-bound cytochromes in *Chloroflexus aurantiacus* studied by EPR, Eur. J. Biochem. 199 (1991) 317–323.
[29] B.D. Bruce, R.C. Fuller, R.E. Blankenship, Primary photochemistry in the facultatively aerobic green photosynthetic bacterium *Chloroflexus aurantiacus*, Proc. Natl Acad. Sci. USA 79 (1982) 6532–6536.
[30] C. Kirmaier, D. Holten, An assessment of the mechanism of initial electron transfer in bacterial reaction centers, Biochemistry 30 (1991) 609–613.
[31] S.I. Yang, J. Li, H.S. Cho, D. Kim, D.F. Bocian, D. Holten, J.S. Lindsey, Synthesis and excited-state photodynamics of phenylethyne-linked porphyrin-phthalocyanine dyads, J. Mater. Chem. 10 (2000) 283–296.
[32] Cohen-BazireG. , SistromW.R. , in: VernonL.P. , SeelyG.R. (Eds.), The Chlorophylls, Academic Press, New York, 1966, pp. 313–341.
[33] S.C. Straley, W.W. Parson, D.C. Mauzerall, R.K. Clayton, Pigment content and molar extinction coefficients of photochemical reaction centers from *Rhodopseudomonas sphaeroides*, Biochim. Biophys. Acta 305 (1973) 597–609.
[34] J.A. Shiozawa, F. Lottspeich, R. Feick, The photochemical reaction center of *Chloroflexus aurantiacus* is composed of two structurally similar polypeptides, Eur. J. Biochem. 167 (1987) 595–600.
[35] P.O.J. Scherer, S.F. Fischer, Model studies to low-temperature optical transitions of photosynthetic reaction centers. II. *Rhodobacter sphaeroides* and *Chloroflexus aurantiacus*, Biochim. Biophys. Acta 891 (1987) 157–164.
[36] H. Vasmel, R.F. Meiburg, H.J.M. Kramer, L.J. de Vos, J. Amesz, Optical properties of the photosynthetic reaction center of *Chloroflexus aurantiacus* at low temperature, Biochim. Biophys. Acta 724 (1983) 333–339.
[37] V.A. Shuvalov, A.Y. Shkuropatov, S.M. Kulakova, M.A. Ismailov, V.A. Shkuropatova, Photoreactions of bacteriopheophytins and bacteriochlorophylls in reaction centers of *Rhodopseudomonas sphaeroides* and *Chloroflexus aurantiacus*, Biochim. Biophys. Acta 849 (1986) 337–346.
[38] G. Venturoli, M. Trotta, R. Feick, B.A. Melandri, D. Zannoni, Temperature dependence of charge recombination from the $P^+Q_A^-$ and $P^+Q_B^-$ states in photosynthetic reaction centers isolated from the thermophilic bacterium *Chloroflexus aurantiacus*, Eur. J. Biochem. 202 (1991) 625–634.
[39] C. Kirmaier, D. Holten, Primary photochemistry of reaction centers from the photosynthetic purple bacteria, Photosynth. Res. 13 (1987) 225–260.
[40] J.I. Chuang, S.G. Boxer, D. Holten, C. Kirmaier, Temperature dependence of electron transfer to the M-side bacteriopheophytin in *Rhodobacter capsulatus* reaction centers, J. Phys. Chem. B 112 (2008) 5487–5499.
[41] N. Woodbury, J. Allen, in: R. Blankenship, M. Madigan, C. Bauer (Eds.), Anoxygenic Photosynthetic Bacteria, Springer Netherlands, Dordrecht, 2004, pp. 527–557.
[42] C.C. Schenck, R.E. Blankenship, W.W. Parson, Radical-pair decay kinetics, triplet yields and delayed fluorescence from bacterial reaction centers, Biochim. Biophys. Acta 680 (1982) 44–59.
[43] A. Ogrodnik, M. Volk, R. Letterer, R. Feick, M.E. Michel-Beyerle, Determination of free energies in reaction centers of *Rb. sphaeroides*, Biochim. Biophys. Acta 936 (1988) 361–371.
[44] E.J. Bylina, C. Kirmaier, L. McDowell, D. Holten, D.C. Youvan, Influence of an amino-acid residue on the optical properties and electron transfer dynamics of a photosynthetic reaction centre complex, Nature 336 (1988) 182–184.
[45] T. Watanabe, M. Kobayashi, in: H. Scheer (Ed.), Chlorophylls, CRC Press, Boca Raton, 1991, pp. 287–315.
[46] E. Katilius, T. Turanchik, S. Lin, A.K.W. Taguchi, N.W. Woodbury, B-Side electron transfer in a *Rhodobacter sphaeroides* reaction center mutant in which the B-Side monomer bacteriochlorophyll is replaced with bacteriopheophytin, J. Phys. Chem. B 103 (1999) 7386–7389.
[47] M. Pudlak, R. Pincak, Electronic pathway in reaction centers from *Rhodobacter sphaeroides* and *Chloroflexus aurantiacus*, J. Biol. Phys. 36 (2010) 273–289.
[48] W.W. Parson, Z.-T. Chu, A. Warshel, Electrostatic control of charge separation in bacterial photosynthesis, Biochim. Biophys. Acta 1017 (1990) 251–272.
[49] P. Hamm, K.A. Gray, D. Oesterhelt, R. Feick, H. Scheer, W. Zinth, Subpicosecond emission studies of bacterial reaction centers, Biochim. Biophys. Acta 1142 (1993) 99–105.
[50] U. Finkele, C. Lauterwasser, W. Zinth, K.A. Gray, D. Oesterhelt, Role of tyrosine M210 in the initial charge separation of reaction centers of *Rhodobacter sphaeroides*, Biochemistry 29 (1990) 8517–8521.
[51] V. Nagarajan, W.W. Parson, D. Gaul, C. Schenck, Effect of specific mutations of tyrosine-(M)210 on the primary photosynthetic electron-transfer process in *Rhodobacter sphaeroides*, Proc. Natl Acad. Sci. USA 87 (1990) 7888–7892.
[52] A.G. Yakovlev, L.G. Vasilieva, A.Y. Shkuropatov, T.I. Bolgarina, V.A. Shkuropatova, V.A. Shuvalov, Mechanism of charge separation and stabilization of separated charges in reaction centers of *Chloroflexus aurantiacus* and of YM210W(L) mutants of *Rhodobacter sphaeroides* excited by 20 fs Pulses at 90 K, J. Phys. Chem. A 107 (2003) 8330–8338.
[53] X. Lin, H.A. Murchison, V. Nagarajan, W.W. Parson, J.P. Allen, J.C. Williams, Specific alteration of the oxidation potential of the electron donor in reaction centers from *Rhodobacter sphaeroides*, Proc. Natl Acad. Sci. USA 91 (1994) 10265–10269.
[54] T.A. Mattioli, X. Lin, J.P. Allen, J.C. Williams, Correlation between multiple hydrogen bonding and alteration of the oxidation potential of the bacteriochlorophyll dimer of reaction centers from *Rhodobacter sphaeroides*, Biochemistry 34 (1995) 6142–6152.
[55] A. Ivancich, K. Artz, J.C. Williams, J.P. Allen, T.A. Mattioli, Effects of hydrogen bonds on the redox potential and electronic structure of the bacterial primary electron donor, Biochemistry 37 (1998) 11812–11820.
[56] R.K. Clayton, B.J. Clayton, Molar extinction coefficients and other properties of an improved reaction center preparation from *Rhodopseudomonas viridis*, Biochim. Biophys. Acta 501 (1978) 478–487.
[57] J.P. Thornber, J.M. Olson, Chlorophyll-proteins and reaction center preparations from photosynthetic bacteria, algae and higher plants, Photochem. Photobiol. 14 (1971) 329–341.
[58] D. Garcia, P. Mathis, A. Verméglio, Kinetics of electron transfer between the tetrahemic cytochrome and the special pair in isolated reaction centers of *Roseobacter denitrificans*, Photosynth. Res. 55 (1998) 331–335.
[59] W. Nitschke, M. Jubault-Bregler, A.W. Rutherford, The reaction center associated tetraheme cytochrome subunit from *Chromatium vinosum* revisited: a reexamination of its EPR properties, Biochemistry 32 (1993) 8871–8879.
[60] W. Nitschke, I. Agalidis, A.W. Rutherford, The reaction-centre associated cytochrome subunit of the purple bacterium *Rhodocyclus gelatinosus*, Biochim. Biophys. Acta 1100 (1992) 49–57.
[61] A. Mulkidjanian, G. Venturoli, A. Hochkoeppler, D. Zannoni, B. Melandri, L. Drachev, Photosynthetic electrogenic events in native membranes of *Chloroflexus aurantiacus*. Flash-induced charge displacements within the reaction center–cytochrome *c*554 complex, Photosynth. Res. 41 (1994) 135–143.